Effect of Convection on a Propagating Front with a Solid Product: Comparison of Theory and Experiments

Gina Bowden,[†] Marc Garbey,[‡] Victor M. Ilyashenko,[†] John A. Pojman,*[,†] Stanislav E. Solovyov,[†] Ahmed Taik,[‡,§] and Vitaly A. Volpert[‡]

Department of Chemistry and Biochemistry, University of Southern Mississippi, Hattiesburg, Mississippi 39406, Laboratoire d'Analyse Numérique, Université Lyon I, Batiment 101, 43, bd du 11 Novembre 1918, 69622 Villeurbanne Cedex, France, and Faculty of Science and Technology, King Hassan II University−Mohammadia, B.P. 146, Mohammadia, Morocco

Received: August 5, 1996; In Final Form: October 21, 1996[⊗]

We studied ascending fronts of acrylamide polymerization in dimethyl sulfoxide in which the reactants in solution are converted to a gel at a higher temperature than the solution. We have calculated the stability boundary (the critical viscosity at which convection occurs) as a function of the front velocity. We found that in a two-dimensional system the presence of walls does stabilize the front compared to an infinite plane, but the shape of the boundary is not affected. Experimental fronts exhibited antisymmetric convection for low viscosities and low front velocities, as predicted by our calculations. However, the experimentally determined boundary differed significantly from the calculated ones, the experimental fronts being more stable. The shapes of the boundaries differ, and we propose this is caused by the temperature dependence of the viscosity, which is not treated in our analysis.

Introduction

Many autocatalytic reactions in solution can sustain a localized reaction front that propagates throughout an unstirred medium.[1] As a front propagates, concentration and thermal gradients are formed that alter the density of the solution, often causing convection. A great deal of work has been done on fronts that propagate in solution via the coupling of mass diffusion with the autocatalytic polynomial reaction kinetics, both experimentally[2−20] and theoretically.[4,21−28]

An extensive body of work has been done on the onset of convection in fronts propagating in vertical orientations in which the stability of the system with respect to the onset of convective fluid flow is essentially independent of the front velocity, and the driving force is the change in composition and not the change in temperature. Pojman et al. considered the problem of the onset of simple convection for ascending fronts with liquid products in terms of the Rayleigh number for the static problem.[10,21] Masere et al. performed a similar analysis and found good agreement with results for the iodate−arsenous acid system for the onset of antisymmetric convection.[4] Numerous other works considered various aspects of the problem.[23−27,29]

Some experimental work has been done on convection that can occur in descending thermal fronts in which a liquid monomer is converted to a solid polymer product.[30,31] In this work we consider the problem of an ascending thermal front with a liquid reactant that is converted to a solid product. The heat released by the chemical reaction can cause the fluid above the front to flow through the interaction of buoyancy, similarly to the Rayleigh−Bénard problem with heating from below.[32] Unlike that situation, the lower boundary is moving (Figure 1). We note that this problem differs from directional solidification in which the low temperature occurs at the solid/liquid interface and the bulk liquid is at the high temperature.[33] Thus the velocity of the front affects the stability of the fluid layer. The precise nature of the interaction between the front and the fluid is the subject of our work.

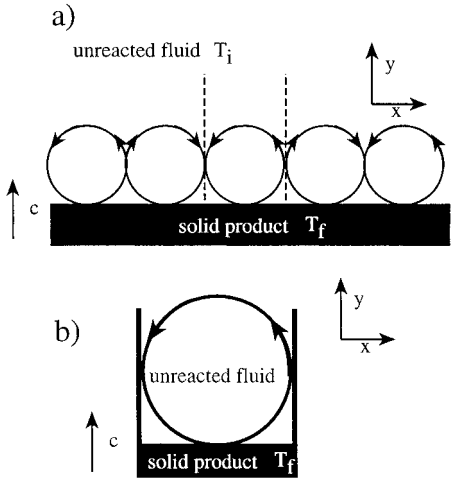

Figure 1. Diagrams of model systems to be studied. A fluid at T_i is converted to a solid product at a final temperature T_f through a propagating front with velocity c. (a) The layer is infinite, and dashed lines indicate length corresponding to the tube diameter of the experimental systems. (b) A two-dimensional system with the walls.

Frontal Polymerization

Most polymerization reactions are exothermic, and under some conditions, localized zones of reaction can propagate through an unstirred system in a process called *frontal polymerization.* Chechilo et al. were the first to study frontal polymerization.[34] They studied methyl methacrylate polymerization in which the liquid monomer was converted to a liquid product. Pojman et al. demonstrated the feasibility of traveling fronts in solutions of thermal free-radical initiators in a variety of neat monomers at ambient pressure using liquid monomers that form polymers with melting points exceeding the reaction temperature of the front.[30,35−37] The field was reviewed in 1984 by Davtyan et al.[38] and recently by Pojman et al.[39] Khan and

[†] University of Southern Mississippi.
[‡] Université Lyon I.
[§] King Hassan II University−Mohammadia.
[⊗] Abstract published in *Advance ACS Abstracts,* January 1, 1997.

S1089-5647(96)02354-1 CCC: $14.00

Pojman have considered the prospects for frontal polymerization in materials synthesis.[40]

We set out to study the stability of ascending fronts of polymerization because convective instabilities pose a significant interference to frontal polymerization and because such fronts are good experimental systems for elucidating the role of convection in thermal fronts. We considered two-dimensional models with and without walls and compared the results with experimental data from test tubes.

Model and Equations

We make the following assumptions in the mathematical formulation of the problem: (1) The reagents are in a cylindrical tube, whose axis is along the gravitational force. The tube is long, and its radius is large enough that we can neglect the walls. We treat the system as an infinite plane. (We will relax this assumption later by including walls.) (2) The chemical reaction is a one-step zero-order reaction. The reaction rate is then given by an expression of this form:

$$W = k(T)\,\varphi(\alpha) \tag{1}$$

where T is the temperature, α is the degree of conversion, and

$$\varphi(\alpha) = \begin{cases} 1 & \text{if } \alpha < 1 \\ 0 & \text{if } \alpha = 1 \end{cases} \tag{2}$$

The temperature dependence of the reaction rate is given by the Arrhenius dependence,

$$k(T) = k_0 \exp(-E/RT) \tag{3}$$

where E is the activation energy, R the ideal gas constant, and k_0 the pre-exponential factor. For the asymptotic analysis we will assume the activation energy is large. (3) The liquid is incompressible. The density of the medium depends on the temperature only, and the change of density is small. (4) The coefficient of mass diffusion is much less than the thermal diffusivity. (5) The reaction product is solid or a gel.

Using these assumptions and the Boussinesq approximation, we have the following system of equations for a two-dimensional plane:

$$\frac{\partial \alpha}{\partial t} = -v\nabla\alpha + k(T)\,\varphi(\alpha) \tag{4}$$

$$\frac{\partial T}{\partial t} = -v\nabla T + \kappa\Delta T + qk(T)\,\varphi(\alpha) \tag{5}$$

$$\frac{\partial v}{\partial t} = -(v\nabla)v + \nu\Delta v + -\frac{1}{\rho}\nabla p + g\beta(T - T_0)\gamma \tag{6}$$

$$\operatorname{div} v = 0 \tag{7}$$

Here $v = (v_x, v_y)$ is the velocity of the medium, p is the pressure, κ is the coefficient of thermal diffusivity, q is the temperature change caused by the reaction ($T_f - T_0$), ρ is the average value of the density, ν is the kinematic viscosity, g is the gravitational acceleration, β is the coefficient of thermal expansion, γ is the unit vector in the z-direction (upward), and

$$\nabla = \left(\frac{\partial}{\partial x}, \frac{\partial}{\partial y}\right), \quad \Delta = \frac{\partial^2}{\partial x^2} + \frac{\partial^2}{\partial y^2}$$

Equations 4−7 describe the heat diffusion, chemical reaction, and the motion of an incompressible fluid. The heat released by the reaction leads to a temperature gradient that can cause a convective instability.

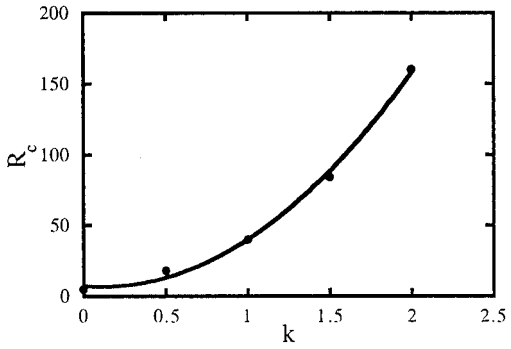

Figure 2. Critical frontal Rayleigh calculated as a function of the wavenumber for an infinite layer with $Pr = 10$.

If we consider a medium at rest, $v = 0$, the system of two equations (4) and (5) describes condensed phase combustion[41] and captures many of the essential aspects of frontal polymerization.[39] The velocity, c, of the stationary front propagation and the temperature distribution can be found by an asymptotic analysis for large Zeldovich numbers:[42]

$$Z = qE/RT_f^2 \tag{8}$$

The velocity can be approximated by an equation derived by Novozhilov:[43]

$$c^2 = \frac{2k_0\kappa RT_f^2}{qE}\exp\left(\frac{-E}{RT_f}\right) \tag{9}$$

A frontal Rayleigh number that determines whether the front is stable can be defined to account for the effect of the front velocity:[44,45]

$$Ra = g\beta q\kappa^2/\nu c^3 \tag{10}$$

It is related to the traditional Rayleigh number for the stability of an infinitely wide fluid layer heated from below by substituting for L the width of the preheat zone, $L = \kappa c^{-1}$:

$$Ra = g\beta qL^3/\nu\kappa \tag{11}$$

Garbey et al. performed the linear stability analysis for this system in an infinite plane.[45] We will not provide the details of the analysis but only explain how we have applied it to a real system. The velocity was scaled by dividing by the value obtained from the infinitely narrow reaction zone approximation with the Novozhilov equation. They calculated the critical frontal Rayleigh number as a function of the Prandtl number ($Pr = \nu/\kappa$) and the dimensionless wavenumber, k,

$$k = 2\pi/\lambda \tag{12}$$

where

$$\lambda = lc/\kappa \tag{13}$$

and c is the dimensional velocity of the front, l is the width of the convective roll, and κ is the thermal diffusivity (see Figure 2). They found that for Prandtl numbers greater than 2, the critical frontal Rayleigh number was only weakly dependent on Pr. Therefore, Pr was fixed at 10. Although the frontal Rayleigh number is only calculated at one dimensionless velocity, the experimental velocity enters through the calculation of the wavenumber.

To prepare a neutral stability boundary, i.e., the curve in the viscosity−velocity plane that demarcates stable and unstable regions of front propagation, the wavenumber of the perturbation

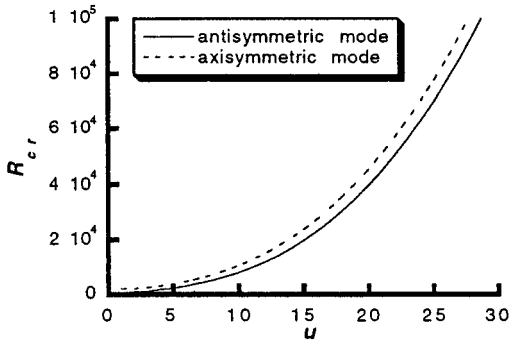

Figure 3. Critical frontal Rayleigh numbers of the antisymmetric and axisymmetric modes for the system with walls as a function of the scaled velocity, u. $Pr = 10$ and $L = 1$.

was calculated from l, which was set equal to the tube diameter. Substituting the relationship between Ra_c and k fit from Figure 2 into the expression for the critical frontal Rayleigh number, we obtain the following relationship between the critical viscosity and the critical velocity:

$$\nu_c = \frac{g\beta q\kappa^2}{5c^3 + 40(2\pi\kappa/D)^2 c} \tag{14}$$

Model with the Effect of Walls

To determine the effect of walls on the stability, we analyzed the same system of equations (4−7) for a bounded two-dimensional plane. (The details of the analysis are presented in the Appendix.) The scaling of the physical width, l, is accomplished by

$$L = cl/2\kappa \tag{15}$$

Figure 3 shows the critical Rayleigh numbers calculated as a function of the scaled velocity for a dimensionless width of 2 ($L = 1$) and a Prandtl number of 10 (again the critical frontal Rayleigh number is insensitive to changes of Pr above $Pr = 2$). Notice how close the values are for the two modes, which are depicted in Figure 4.

To calculate the critical frontal Rayleigh for different dimensional velocities, we calculate L using eq 15 and calculate the dimensionless velocity $\tilde{u}$ by

$$\tilde{u} = L\sqrt{2} \tag{16}$$

Using this $\tilde{u}$, we calculate the critical frontal Rayleigh number, $\tilde{Ra}$, from the graph in Figure 3 and substitute into eq 10 to obtain

$$\nu_c = g\beta q\kappa^2\left(\frac{L}{c}\right)^3 \frac{1}{\tilde{Ra}} \tag{17}$$

For the case with walls we calculated the streamline functions for the first two modes, shown in Figure 4. The first mode to appear is an antisymmetric fluid motion, and the second is axisymmetric, the same as observed in a nonreacting fluid.

Choice of the Experimental System

We have assumed that the only change in density occurs from thermal expansion. Because there are significant isothermal density changes in polymerization reactions (as large as 25%), fronts with liquid polymers disintegrate due to the Rayleigh−Taylor instability.[39,46,47] Thus, they are not suitable candidates for studying simple convective instabilities.

Fronts that produce solid products, such as methacrylic acid and triethylene glycol dimethacrylate, could be studied. However, bubbles that are formed from by-products of the initiators interfere with ascending fronts.[36,39] The bubbles rise from the front, causing fluid motion that obscures any convection caused by the front itself. Bubbles can be suppressed by performing the fronts in a pressure reactor,[39] but this is difficult.

Fronts of epoxy curing can be used (with BCl_3−amine complex as the curing agent),[39] but the epoxy resin's viscosity can change by 2 orders of magnitude from the initial to the front temperature, and the velocity can only be varied from 0.5 to 1 cm/min. At higher concentrations of the BCl_3−amine complex the formation of bubbles prevents reliable front velocity measurements.

Pojman et al. recently developed an ideal system that is bubble-free. Fronts with acrylamide (and a small amount of bisacrylamide to cross-link the product and prevent fingering) dissolved in dimethyl sulfoxide (DMSO) with potassium persulfate as the initiator are excellent for studying convection because there are no bubbles and the front velocity can be varied from 0.5 to 2.5 cm/min.[48]

Comparison of Assumptions of the Model with the Physical System

(1) The reaction zone is infinitely narrow; that is, the concentration profile of the product is a step function. Figure 5 shows a temperature profile of a convection-free front. Because gelation occurs at much less than complete conversion, the maximum temperature (167 °C) occurs not at the solid−liquid interface but rather 2 mm behind the gel point. Because no convection can occur in the gelled medium, we used the temperature at the interface (75 °C) to calculate the q in our calculations.

(2) The viscosity is independent of temperature. The viscosity of the medium is certainly a function of temperature, as seen in Figure 6, varying as much as a factor of 20 from 25 to 75 °C. We used the viscosities measured at the interface temperature and the initial temperature in our comparisons.

(3) The thermal diffusivity is independent of temperature and conversion. This appears to be a reasonable assumption, as we will see below, where we calculate the κ from the temperature profile.

Experimental Section

All chemicals were used as received: potassium persulfate, *N*,*N*-methylenebisacrylamide, and acrylamide (99%) from Aldrich; dimethyl sulfoxide from Fisher; and Cab-O-Sil amorphous fumed silica from Cabot Corporation.

Stability and Velocity Measurements. The system consisted of acrylamide dissolved in dimethyl sulfoxide (DMSO). The initiator, potassium persulfate, was used along with hydroquinone to inhibit homogeneous polymerization and *N*,*N*-methylenebisacrylamide to cross-link the polymer. The concentration of acrylamide was 1:1 w/v. The *N*,*N*-methylenebisacrylamide concentration was 1% w/v of the total solution. The amount of hydroquinone used was 0.10 g for every 64 mL of DMSO. Such a small amount of hydroquinone was used because higher hydroquinone concentrations affect the velocity of the front. The amount of initiator used was varied in order to change the velocity of the front. The concentration was usually between 0.5% and 2.5% of solution.

Amorphous fumed silica (Cab-O-Sil) was added to vary the viscosity of the system. The amount used ranged between 2% and 3% of the solution. Once the Cab-O-Sil was added, the mixture had to be briefly degassed in order to properly mix the Cab-O-Sil with the solution. The mixture was placed in a 16 × 150 mm borosilicate culture tube (Fisher). For reasons we

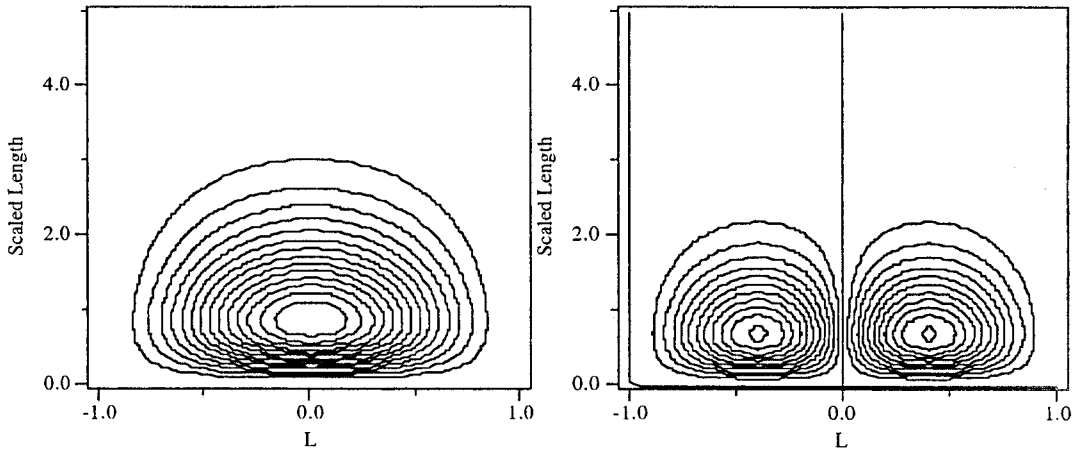

Figure 4. (a) Streamlines for the first unstable mode (antisymmetric) calculated for the plane with walls. $Pr = 10$. Fluid motion is clockwise. (b) Streamlines for the second unstable mode (axisymmetric). $Pr = 10$. Fluid motion is clockwise on the left side and counterclockwise on the right.

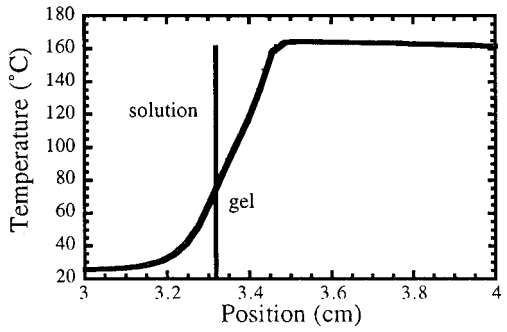

Figure 5. Temperature profile for 0.89 cm/min front with 3% Cab-O-Sil. The line indicates the transition from solution to gel, which occurs at 75 °C.

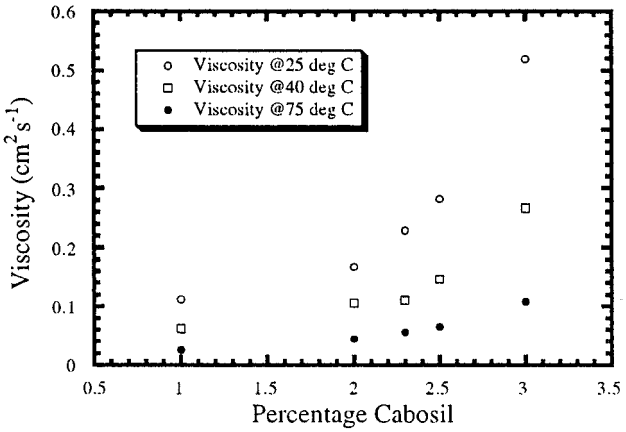

Figure 6. Viscosity of a 1:1 acrylamide/DMSO solution as a function of the Cab-O-Sil content, at three different temperatures.

do not know, the Cab-O-Sil increased the rate of homogenous polymerization, i.e., reduced the pot life.

Initially, heat was applied to the mixture to start the front with a soldering iron in contact with the solution or through the glass. For an ascending front, some solution without Cab-O-Sil was added to a small amount of 400 μm Glas-Shot (Cataphote) in the bottom of the tube. The mixture with Cab-O-Sil was added on top of this. The front was first ignited in the Glas-Shot mixture. This allowed the Cab-O-Sil mixture front to be ignited by the flat surface of the Glas-Shot front. After the front was initiated, the tube was inserted into a side-armed 250 mL Erlenmeyer flask with a rubber gasket and evacuated. This procedure was done in order to eliminate external convection of the air surrounding the tube. Each ascending and descending front was videotaped with a Cohu High Performance CCD camera.

Viscosity Measurements. To measure the viscosity of the mixtures, Cannon-Fenske routine viscometers were used. For the Cab-O-Sil 2% mixture, a size 200 Cannon-Fenske viscometer was used. For all of the other mixtures a size 300 viscometer was used. These viscometers were not necessarily used for their designated viscosity range but for their capillary size. The Cab-O-Sil tended to block the viscometers with smaller capillaries. To determine if using a viscometer that was out of the viscosity range of the liquid made a large difference in the measurement, the viscosity of pure dimethyl sulfoxide was measured using the size 200 Cannon-Fenske viscometer. The viscosity measurement had a 4.5% difference from the accepted value of dimethyl sulfoxide viscosity.

To measure viscosity, the viscometer was charged with the mixture. The viscometer was then placed in a water bath of 75 $\pm$ 0.1 °C and allowed to equilibrate for 15 min. A stopwatch was then used to measure the time needed for the liquid to move through the capillary. Three time measurements were recorded for each mixture. These measurements were averaged, and this time was multiplied by the viscometer constant provided by the manufacturer at 75 °C. (The gel point of the front is 80 °C, but it was difficult to maintain our water bath above 75 °C.) We ignored this small effect on the viscosity. The preceding procedure was also followed to obtain the viscosities at 40 and 25 °C.

Front Temperature, Density, and Thermal Expansion Coefficient Measurements. The temperature of the front was obtained using an unsheathed Omega thermocouple (6 in., part TMQSS-020G-6). This thermocouple was formed into a spiral parallel with the front and placed in a test tube containing the mixture. The thermocouple was attached to an Omega thermocouple thermometer. The run was videotaped in order to observe the location of the front and the thermometer display simultaneously. This was done three times, and the average gel point was found to be 75 $\pm$ 5 °C.

It was determined that the mixture without Cab-O-Sil has a density of 1.18 g cm^{-3} at 25 °C. The density was again measured as a function of temperature in order to determine the thermal expansion coefficient. For these measurements, a 50 mL pycnometer and a water bath were used. At room temperature, the pycnometer was filled with the solution and weighed. The pycnometer with solution was then heated, and the solution was allowed to overflow as it expanded. When the next desired temperature was reached, the pycnometer and solution were reweighed. This procedure was followed for four

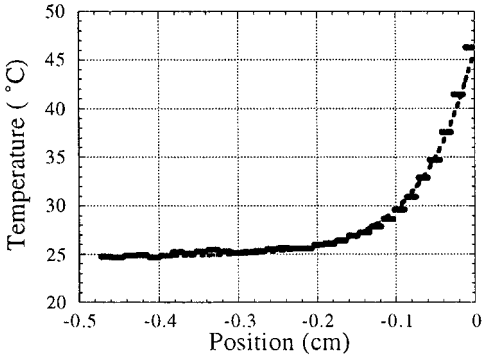

Figure 7. Temperature profile for 0.89 cm/min front with 3% Cab-O-Sil. From a fit (dashed line) of eq 19 to the data, the thermal diffusivity was calculated to be 0.06 cm^2 min^{-1}.

temperatures. Then the density at each temperature was calculated to be 1.18 g/cm^3 at 25 °C; 1.16 g/cm^3 at 42 °C; 1.15 g/cm^3 at 62 °C; and 1.13 g/cm^3 at 75 °C. To determine the thermal expansion coefficient, the collected data and the following equation were used:[21]

$$\beta = (\Delta V/V_i)/\Delta T \tag{18}$$

where β is the thermal expansion coefficient, V_i is the initial volume, ΔV is the change in volume, and ΔT is the change in temperature. A thermal expansion coefficient value was calculated for each of the three changes in temperature. The thermal expansion coefficient is 9.9×10^{-4} $°C^{-1}$.

Criteria for Determining Stability. Unstable ascending fronts propagate faster than stable ones. Thus, it should be possible to compare the velocity of an ascending and descending front with the same viscosity to determine the stability. However, near the stability boundary the velocities are nearly identical (within a few percent). Therefore, we injected a drop of bromophenol/DMSO solution above the front. If the blue solution moved as the front propagated upward, the front was counted as unstable.

Determination of the Thermal Diffusivity. We estimated the thermal diffusivity of the acrylamide/DMSO/Cab-O-Sil mixture from the temperature profile from the relationship between the front velocity (c), temperature profile, and thermal diffusivity:[42]

$$T(x) = T_0 + \Delta T \exp(cx/\kappa) \tag{19}$$

Figure 7 shows the fit that provides a value for $\kappa = 0.06$ cm^2 min^{-1} (1×10^{-4} cm^2 s^{-1}).

Results

Descending fronts are always flat, but the shapes of ascending fronts depend on the velocity and viscosity. If the viscosity and/or velocity are large enough, the ascending front is flat. If we fix the velocity at 2.6 cm/min and decrease the viscosity, at a critical value (0.04 cm^2 s^{-1}) the ascending front will become slightly distorted, as seen in Figure 8. The fluid above the front moves in an antisymmetric roll. The front velocity is only a few percent faster than the descending front, but the fluid velocity in the convective roll can be significant (on the order of 1 cm/min). This corresponds to the streamlines shown in Figure 4a.

As the viscosity is decreased further (0.025 cm^2 s^{-1}), a new mode of convection occurs. Figure 9 shows an axisymmetric front that propagates much faster than its descending version (2.63 cm/min versus 6.11 cm/min). This corresponds to the streamlines shown in Figure 4b. This sequence of convective

Figure 8. Ascending front with 1% Cab-O-Sil (ν at 75 °C = 0.045 cm^2 s^{-1}) and a velocity of 1.5 cm min^{-1}), which exhibits antisymmetric convection with the fluid rising on the left and sinking on the right.

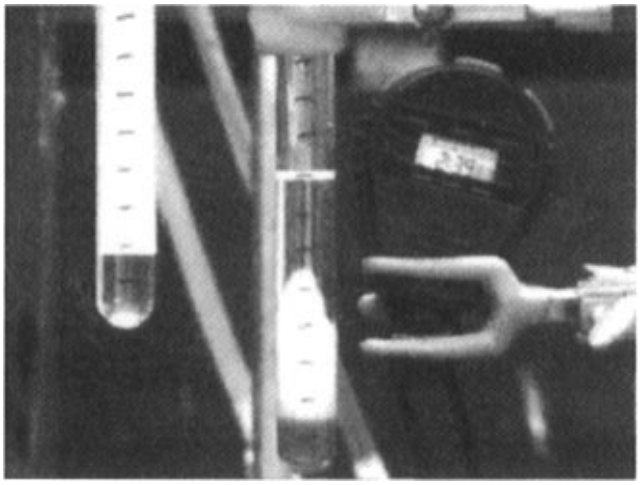

Figure 9. Axisymmetric convection in an ascending front. Front on the left is descending with a velocity of 2.63 cm/min. Front on the right exhibits axisymmetric convection, and the front propagates with a velocity of 6.11 cm/min. System contains 1% Cab-O-Sil.

modes is the same as observed in ascending fronts in the iodate−arsenous acid system.[4,10]

By analyzing the behavior of 33 ascending fronts, we determined a stability boundary, which is shown in Figure 10. We have estimated the exact position of the boundary between fronts that were stable and the next one at the same viscosity but a different velocity. For the two highest viscosities it was not possible to have a slower front without homogeneous reaction. Thus, we can only say for those viscosities that the boundary cannot occur at higher front velocities. The results are shown for the viscosities measured at 75 °C. Although we did not map out the complete boundary between the antisymmetric mode and the axisymmetric one, the one point we measured is consistent with the stability analysis in that the axisymmetric mode is quite close to the boundary between a planar and antisymmetrically shaped front.

Figure 11 shows a comparison of the experimental boundaries (using viscosities at 26 and 75 °C) with those calculated for an infinite plane and a bounded plane.

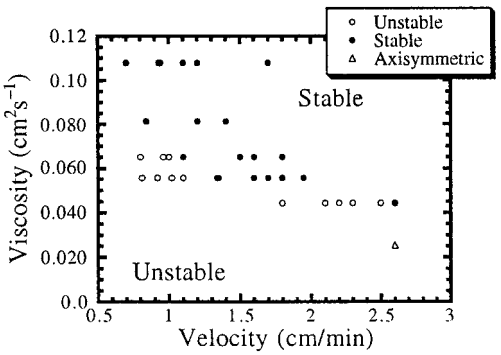

Figure 10. Experimental data on ascending fronts. Viscosities were measured at 75 °C.

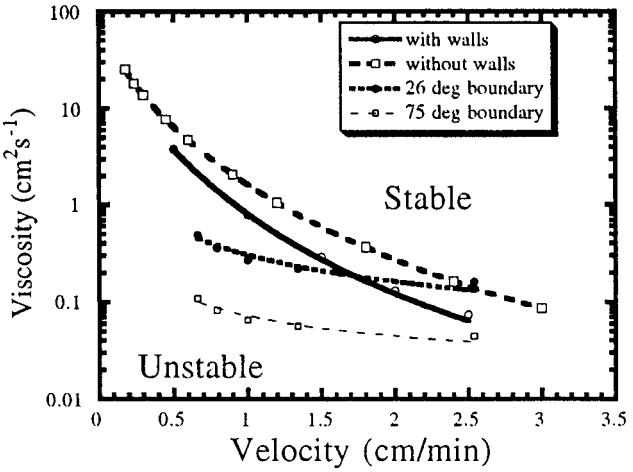

Figure 11. Comparison of experimental stability diagram and calculated without walls. The following parameters were used in the calculations: $\beta = 9.94 \times 10^{-4}$ K^{-1}; q = 58 K; $\kappa = 0.06$ cm^{2}min^{-1}.

A curve of the form

$$\nu_c = a + bc^{-1} \tag{20}$$

was fit to the experimental boundaries, where a and b are free parameters and c is the experimental velocity. ($1/c^2$ and $1/c^3$ did not fit.) We attempted to fit the boundary with a function of form of the boundary without walls, where a_1, a_2, and a_3 are free parameters,

$$\nu_c = a_1/(a_2c^3 + a_3c) \tag{21}$$

but it did not fit as well as eq 20. This curve was fit to the boundary calculated with walls.

Discussion

Although the frontal Rayleigh number has the analogy with the traditional Rayleigh number (eq 11) because the preheat zone can be considered as the height of the fluid layer in the classical problem, there is a significant difference. In Figure 5 we can see that the preheat zone is about 0.3 cm. In the classical Rayleigh−Bénard configuration,[32] the convective rolls could be no larger than this size because of the upper boundary. The convective rolls caused by the front in Figure 8 were about 3 cm high.

The experimentally measured velocities of ascending fronts with antisymmetric convection are almost the same as the descending ones, while axisymmetric convection significantly increases the front velocity. We do not know why the two modes have such a different effect on the front.

It is interesting to see that the inclusion of walls in the calculation does stabilize the front but does not change the dependence of the critical viscosity on the velocity. Also, the critical viscosity dependence on the velocity is not just to c^{-3}, as might be expected from the frontal Rayleigh number in eq 10, but shows the dependence of the form in eq 21. This is because the critical frontal Rayleigh number is itself a function of the velocity.

The experimentally determined stability boundary in Figure 10 differs from both calculated ones in two ways. The experimental boundary is lower in the plane than the calculated boundaries, which means the experimental fronts are more stable than predicted. Errors in the determination of q, β, or κ would cause a shift in the boundary along the y-axis without changing the dependence of the critical viscosity on the front velocity. More important is the difference in functional dependence of the boundary. Both the calculated boundaries have the form of eq 21, but the experimental one shows a weaker dependence on the velocity.

We consider several possible reasons why the calculated boundary does not agree with the experimental data.

(1) The ΔT is a function of the front velocity. We measured the temperature profile for a front with 0.89 cm/min velocity. The overall temperature change is lower than that for the 1.7 cm/min front, but the temperature at which the gel forms is still 75 °C.

(2) There is a systematic error in viscosity measurements. The fluid is non-Newtonian and probably is a Bingham plastic at high concentrations, meaning it possesses an infinite viscosity up to a critical shear.[49] However, at the low Cab-O-Sil concentrations used, the fluid flows readily. The fluid flows observed in the viscometer were on the same order as those observed in the convective rolls (about 1 cm/min).

(3) The thermal diffusivity, κ, is a function of T and/or conversion. However, we successfully fit the temperature profile to obtain κ.

(4) The viscosity is temperature dependent. We believe that this is the most significant cause for the deviation of the calculated boundary from experimental ones. Future work should include this effect and a calculation and experimental determination of the boundary between the two modes.

Conclusions

We have calculated the stability boundary (the critical viscosity at which an ascending front becomes unstable) as a function of the front velocity. We found that in a plane the presence of walls does stabilize the front compared to an infinite plane, but the shape of the boundary is not affected. The experimentally determined boundaries differ significantly from the calculated ones, the experimental fronts being more stable, but the qualitative trend is the same. The difference between the boundaries could be caused by uncertainty in the constants used in the calculations. The shapes of the boundaries differ, and we propose this is caused by the temperature dependence of the viscosity, which is not treated in our analysis.

Acknowledgment. This work was supported by the National Science Foundation (CTS-9319175 and the Mississippi EPSCoR program) and by the Air Force Office of Scientific Research. J.A.P. gratefully acknowledges the support received from the Laboratoire d'Analyse Numerique Université Lyon I during his stay. We also thank Roger Hester and the Cabot Corporation for helpful discussions.

Appendix: Linear Stability Analysis of System with Walls

Following the linear stability analysis[45] of the system (4)-(7), we consider the eigenvalue problem for the streamline function ψ and the dimensionless temperature ϑ:

$$\begin{cases} Pr\Delta\Delta\psi + u\frac{\partial}{\partial z}\Delta\psi - \omega\Delta\psi + Q\frac{\partial\vartheta}{\partial x} = 0 \\ \Delta\vartheta + u\frac{\partial\vartheta}{\partial z} - \omega\vartheta - \vartheta_s'(z)\frac{\partial\psi}{\partial x} = 0 \end{cases} \quad (A.1)$$

$$-1 \le x \le 1,\ z \ge 0$$

with boundary conditions

$$x = -1, 1;\quad z = 0, \infty;\quad \frac{\partial\psi}{\partial x} = \frac{\partial\psi}{\partial z} = 0$$

$$x = -1, 1;\quad \frac{\partial\vartheta}{\partial x} = 0 \quad (A.2)$$

$$z = 0:\ \frac{\partial\vartheta}{\partial z} = -u\vartheta \qquad z = \infty:\ \vartheta = 0$$

where prime denotes the derivative with respect to the z-coordinate, Pr is the Prandtl number:

$$Pr = \nu/\kappa$$

$$Q = PrRa$$

and Ra is the frontal Rayleigh number:

$$Ra = g\beta q\kappa^2/\nu c^3$$

Here, c is dimensional front velocity, and u is the dimensionless front velocity. The solution is found in the following form:

$$\psi(x,z) = \sum_{i=0}^{\infty}\phi_i(x)\, a_i(z) \quad (A.3)$$

$$\vartheta(x,z) = \sum_{i=0}^{\infty}\tau_i(x)\, b_i(z) \quad (A.4)$$

with the conditions

$$a_i(0) = a_i'(0) = 0 \quad (A.5)$$

$$b_i'(0) + ub_i(0) = 0$$

Here ϕ_i and τ_i are the eigenfunctions of the corresponding operators in the section of a cylinder: $\phi_i(x)$ are the eigenfunctions of the problem

$$\tilde{\Delta}^2\phi + \lambda\tilde{\Delta}\phi = 0 \quad (A.6)$$

$$\phi(\pm1) = \phi'(\pm1) = 0 \quad (A.7)$$

The even eigenfunctions are

$$\phi_i(x) = \frac{1}{\sqrt{I_i}}\left[\frac{\cosh kx}{\cosh k} - \frac{\cos x\sqrt{\lambda_i - k^2}}{\cos\sqrt{\lambda_i - k^2}}\right],\quad i = 0, 2, 4, ... \quad (A.8)$$

$$I_i = \frac{\lambda_i}{2(k^2 - \lambda_i)}(k^2 + k\tanh k - k^2\tanh^2 k - \lambda_i) \quad (A.9)$$

$$\sqrt{\lambda_i - k^2}\tan\sqrt{\lambda_i - k^2} = -k\tanh k \quad (A.10)$$

and the odd eigenfunctions are

$$\phi_i(x) = \frac{1}{\sqrt{I_i}}\left[\frac{\sinh kx}{\sinh k} - \frac{\sin x\sqrt{\lambda_i - k^2}}{\sin\sqrt{\lambda_i - k^2}}\right],\quad i = 1, 3, 5, ... \quad (A.11)$$

$$I_i = \frac{\lambda_i}{2(k^2 - \lambda_i)}(k^2 + k\coth k - k^2\coth^2 k - \lambda_i) \quad (A.12)$$

$$\sqrt{\lambda_i - k^2}\cot\sqrt{\lambda_i - k^2} = -k\coth k \quad (A.13)$$

Here

$$\int_{-1}^{1}\phi_i\tilde{\Delta}\phi_k\, dx = -\delta_{ik} \quad (A.14)$$

$$\tilde{\Delta} = \frac{\partial^2}{\partial x^2} - k^2 \quad (A.15)$$

and k is the wavenumber in the y-direction. Now, $\tau_i(x)$ are the eigenfunctions of the problem:

$$\tau'' + \mu\tau = 0 \quad (A.16)$$

$$\tau'(\pm1) = 0 \quad (A.17)$$

The even eigenfunctions are

$$\tau_i(x) = \cos\frac{\pi x}{2}i,\quad i = 0, 2, 4, ... \quad (A.18)$$

and the odd eigenfunctions are

$$\tau_i(x) = \sin\frac{\pi x}{2}i,\quad i = 1, 3, 5, ... \quad (A.19)$$

here

$$\sqrt{\mu_i} = \pi i/2 \quad (A.20)$$

and

$$\int_{-1}^{1}\tau_i\tau_k\, dx = 0,\quad i \ne k \quad (A.21)$$

Then the equations for the streamlines and the temperature take the form

$$Pr(a_i^{iv} - 2\lambda_i a_i'' + \lambda_i^2 a_i) + u(a_i''' - \lambda_i a_i') - \omega(a_i'' - \lambda_i a_i) - Q\sum_{j=0}^{\infty}\sigma_{ij}b_j(z) = 0 \quad (A.22)$$

$$b_i'' + ub_i' - (\mu_i + \omega)b_i + \frac{u}{\mu_i}e^{-uz}\sum_{j=0}^{\infty}\sigma_{ji}a_j(z) = 0 \quad (A.23)$$

We limit our stability analysis to the first term of the infinite sum by j. We also take $\omega = 0$. It corresponds to the cellular instability where the front is curved, but its shape as well as the whole convective structure does not depend on time. (Periodic in time or pulsating instability appears if ω is imaginary.) In this case the eigenvalue problem (A.1) takes the form

$$\begin{cases} Pr(v^{iv} - 2\lambda v'' + \lambda^2 v) + u(v''' - \lambda v') - Q\sigma_1\vartheta = 0 \\ \vartheta'' + u\vartheta' - \mu\vartheta + \dfrac{u}{\mu}\sigma_2 e^{-uz} v = 0 \end{cases} \tag{A.24}$$

for $0 \le z \le \infty$, and σ_1, σ_2, λ, and μ are constants.

We look for the solution in the form of series

$$v = \sum_{j=0}^{\infty} j e^{\tau_j z}, \quad \vartheta = \sum_{j=0}^{\infty} m_j e^{\tau_j z} \tag{A.25}$$

From the analysis[45] there are three different cases corresponding to three linearly independent solutions of (A.24) bounded at infinity.

First case:

$$\tau_1 = -\frac{u}{2} - \sqrt{\frac{u^2}{4} + \mu}, \quad \tau_j = \tau_{j-1} - u, \quad j = 2, 3, \ldots$$

$$m_1 = 1$$

$$m_j = \frac{-\dfrac{u}{\mu}\sigma_2 k_{j-1}}{\tau_j^2 + u\tau_j - \mu}, \quad j = 2, 3, \ldots \tag{A.26}$$

$$k_j = \frac{Q\sigma_1 m_j}{(\tau_j^2 - \lambda)(Pr\tau_j^2 + u\tau_j - Pr\lambda)}, \quad j = 1, 2, \ldots$$

Second case:

$$\tau_1 = -\sqrt{\lambda}, \quad \tau_j = \tau_{j-1} - u, \quad j = 2, 3, \ldots$$

$$m_1 = 0$$

$$m_j = \frac{-\dfrac{u}{\mu}\sigma_2 k_{j-1}}{\tau_j^2 + u\tau_j - \mu}, \quad j = 2, 3, \ldots \tag{A.27}$$

$$k_j = \frac{Q\sigma_1 m_j}{(\tau_j^2 - \lambda)(Pr\tau_j^2 + m\tau_j - Pr\lambda)}, \quad j = 1, 2, \ldots$$

Third case:

$$\tau_1 = -\frac{u}{2Pr} - \sqrt{\frac{u^2}{4Pr^2} + \lambda}, \quad \tau_j = \tau_{j-1} - u, \quad j = 2, 3, \ldots$$

$$m_1 = 0$$

$$m_j = \frac{-\dfrac{u}{\mu}\sigma_2 k_{j-1}}{\tau_j^2 + u\tau_j - \mu}, \quad j = 2, 3, \ldots \tag{A.28}$$

$$k_j = \frac{Q\sigma_1 m_j}{(\tau_j^2 - \lambda)(Pr\tau_j^2 + u\tau_j - Pr\lambda)}, \quad j = 1, 2, \ldots$$

Let us denote the particular solutions corresponding to the cases 1−3 by (v_1,ϑ_1), (v_2,ϑ_2), (v_3,ϑ_3), respectively. Then the general solution is

$$V = c_1 v_1 + c_2 v_2 + c_3 v_3 \tag{A.29}$$

$$\Theta = c_1\vartheta_1 + c_2\vartheta_2 + c_3\vartheta_3$$

and the boundary conditions are

$$V(0) = V'(0) = 0, \quad \Theta'(0) + u\Theta(0) = 0 \tag{A.30}$$

Then the linear system of equations results in

$$\begin{cases} c_1 v_1(0) + c_2 v_2(0) + c_3 v_3(0) = 0 \\ c_1 v_1'(0) + c_2 v_2'(0) + c_3 v_3'(0) = 0 \\ c_1(\vartheta_1'(0) + u\vartheta_1(0)) + c_2(\vartheta_2'(0) + u\vartheta_2(0)) + \\ \qquad c_3(\vartheta_3'(0) + u\vartheta_3(0)) = 0 \end{cases} \tag{A.31}$$

and the condition

$$\det\begin{pmatrix} v_1(0) & v_2(0) & v_3(0) \\ v_1'(0) & v_2'(0) & v_3'(0) \\ \vartheta_1'(0) + u\vartheta_1(0) & \vartheta_2'(0) + u\vartheta_2(0) & \vartheta_3'(0) + u\vartheta_3(0) \end{pmatrix} = 0 \tag{A.32}$$

gives the critical Rayleigh number corresponding to the stability boundary.

Numerical Methods

Equation A.32 with expressions A.25−A.28 was solved for different parameter values of *Pr* and *u* resulting in critical Rayleigh numbers Ra_c. The solution algorithm involved the calculation of the determinant (A.32) for a set of *Ra* values (for example, from 0 to 10^6), and when the sign of the determinant changed, the exact solution was found in the interval by consecutively dividing the *Ra* step by half until a given precision of the root was reached. If more than one root was found, the lowest value of *Ra* was considered to be the critical Rayleigh number. Sometimes the singular solutions were found (i.e., the determinant (A.32) changed sign through infinity). These solutions were excluded from our consideration.

Results and Discussion

As follows from the linear stability analysis for the first unstable mode, the following values of constants are be taken:

$$\sigma_1 = \sigma_2 = -2\pi/3, \quad \mu = \pi^2/4, \quad \lambda = \pi^2 \tag{A.33}$$

While for the second unstable mode we used the following values:

$$\sigma_1 = \sigma_2 = -2\pi^2\sqrt{\lambda}/(\lambda - \pi^2), \quad \mu = \pi^2 \tag{A.34}$$

and the first positive root of the equation $\tan(\sqrt{\lambda}) = \sqrt{\lambda}$ for λ. When *Ra* critical was calculated for a series of Prandtl numbers *Pr* using constants from (A.33) and (A.34), we compared the stability of both modes. Lower critical Rayleigh numbers for the first mode mean this instability appears first as we increase the Rayleigh number by decreasing the initial solution viscosity or the front velocity (see Figure 2). To calculate the eigenfunctions corresponding to zero eigenvalue (critical frontal Rayleigh number), we used the following formulas:[45]

$$\psi(x,z) = v(z)(1 + \cos(\pi x))/\pi \tag{A.35}$$

$$\vartheta(x,z) = \vartheta(z)\sin(\pi x/2)$$

The first component here is the stream function ψ, and the second one is the dimensionless temperature ϑ. The level lines of the stream function give the lines along which the liquid moves. Figure 4 shows the streamlines of the fluid motion and corresponding temperature fields for both calculated modes.

These pictures exactly match the experimental observations of convection in ascending polymerization fronts.

References and Notes

(1) Ross, J.; Müller, S. C.; Vidal, C. *Science* **1988**, *240*, 460−465.

(2) Nagypál, I.; Bazsa, G.; Epstein, I. R. *J. Am. Chem. Soc.* **1986**, *108*, 3635−3640.

(3) Bazsa, G.; Epstein, I. R. *J. Phys. Chem.* **1985**, *89*, 3050−3053.

(4) Masere, J.; Vasquez, D. A.; Edwards, B. F.; Wilder, J. W.; Showalter, K. *J. Phys. Chem.* **1994**, *98*, 6505−6508.

(5) Plesser, T.; Wilke, H.; Winters, K. H. *Chem. Phys. Lett.* **1992**, *200*, 158−162.

(6) Nagy, I. P.; Pojman, J. A. *J. Phys. Chem.* **1993**, *97*, 3443−3449.

(7) Tzalmona, A.; Armstrong, R. L.; Menzinger, M.; Cross, A.; Lemaire, C. *Chem. Phys. Lett.* **1992**, *188*, 457−461.

(8) Miike, H.; Müller, S. C.; Hess, B. In *Cooperative Dynamics in Physical Systems*; Takayama, H., Ed.; Springer-Verlag: Berlin, 1989; pp 328−329.

(9) Hauser, M. J. B.; Simoyi, R. H. *Phys. Lett. A* **1994**, *191*, 31−38.

(10) Pojman, J. A.; Epstein, I. R.; McManus, T.; Showalter, K. *J. Phys. Chem.* **1991**, *95*, 1299−1306.

(11) Pojman, J. A.; Epstein, I. R.; Nagy, I. *J. Phys. Chem.* **1991**, *95*, 1306−1311.

(12) Pojman, J. A. *J. Chem. Educ.* **1990**, *67*, 792−794.

(13) Nagy, I. P.; Keresztessy, A.; Pojman, J. A. *J. Phys. Chem.* **1995**, *99*, 5385−5388.

(14) Nagy, I. P.; Keresztessy, A.; Pojman, J. A.; Bazsa, G.; Noszticzius, Z. *J. Phys. Chem.* **1994**, *98*, 6030−6037.

(15) Keresztessy, A.; Nagy, I. P.; Bazsa, G.; Pojman, J. A. *J. Phys. Chem.* **1995**, *99*, 5379−5384.

(16) Matthiessen, K.; Müller, S. C. *Phys. Rev. E* **1995**, *52*, 492−495.

(17) Miike, H.; Müller, S. C.; Hess, B. *Chem. Phys. Lett.* **1988**, *144*, 515−0520.

(18) Miike, H.; Müller, S. C.; Hess, B. *Phys. Rev. Lett.* **1988**, *61*, 2109−2112.

(19) Miike, H.; Yamamoto, H.; Kai, S.; Müller, S. C. *Phys. Rev. E* **1993**, *48*, 1627−1630.

(20) Plesser, T.; Miike, H.; Müller, S. C.; Winters, K. H. In *Spatial Inhomogeneities and Transient Behavior in Chemical Kinetics*; Gray, P., Nicolis, G., Baras, F., Borckmans, P., Scott, S. K., Eds., Manchester University Press: Manchester, U.K., 1990; pp 383−391.

(21) Pojman, J. A.; Epstein, I. R. *J. Phys. Chem.* **1990**, *94*, 4966−4972.

(22) Vasquez, D. A.; Edwards, B. F.; Wilder, J. W. *Phys. Rev. A* **1991**, *43*, 6694−6699.

(23) Vasquez, D. A.; Wilder, J. W.; Edwards, B. F. *Phys. Fluids A* **1992**, *4*, 2410−2414.

(24) Vasquez, D. A.; Wilder, J. W.; Edwards, B. F. *J. Chem. Phys.* **1993**, *98*, 2138−2143.

(25) Vasquez, D. A.; Littley, J. M.; Wilder, J. W.; Edwards, B. F. *Phys. Rev. E* **1994**, *50*, 280−284.

(26) Vasquez, D. A.; Edwards, B. F.; Wilder, J. W. *Phys. Fluids* **1995**, *7*, 2513−2516.

(27) Wu, Y.; Vasquez, D. A.; Edwards, B. F.; Wilder, J. W. *Phys. Rev. E* **1995**, *51*, 1119−1127.

(28) Wilder, J. W.; Vasquez, D. A.; Edwards, B. F. *Phys. Rev. E* **1993**, *47*, 2138−2143.

(29) Wilder, J. W.; Edwards, B. F.; Vasquez, D. A.; Sivashinsky, G. I. *Physica D* **1994**, *73*, 217−226.

(30) Pojman, J. A.; Craven, R.; Khan, A.; West, W. *J. Phys. Chem.* **1992**, *96*, 7466−7472.

(31) Nagy, I. P.; Pojman, J. A. *J. Phys. Chem.* **1996**, *100*, 3299−3304.

(32) Cross, M. C.; Hohenberg, P. C. *Rev. Mod. Phys.* **1993**, *65*, 851−1112.

(33) Davis, S. H.; Müller, U.; Dietsche, C. *J. Fluid Mech.* **1984**, *144*, 133−151.

(34) Chechilo, N. M.; Khvilivitskii, R. J.; Enikolopyan, N. S. *Dokl. Akad. Nauk SSSR* **1972**, *204*, 1180−1181.

(35) Pojman, J. A. *J. Am. Chem. Soc.* **1991**, *113*, 6284−6286.

(36) Pojman, J. A.; Willis, J.; Fortenberry, D.; Ilyashenko, V.; Khan, A. *J. Polym. Sci. Part A: Polym Chem.* **1995**, *33*, 643−652.

(37) Pojman, J. A.; Willis, J. R.; Khan, A. M.; West, W. W. *J. Polym. Sci. Part A: Polym Chem.* **1996**, *34*, 991−995.

(38) Davtyan, S. P.; Zhirkov, P. V.; Vol'fson, S. A. *Russ. Chem. Rev.* **1984**, *53*, 150−163.

(39) Pojman, J. A.; Ilyashenko, V. M.; Khan, A. M. *J. Chem. Soc., Faraday Trans.* **1996**, *92*, 2825−2837.

(40) Khan, A. M.; Pojman, J. A. *Trends Polym. Sci. (Cambridge, U.K.)* **1996**, *4*, 253−257.

(41) Merzhanov, A. G.; Khaikin, B. I. *Prog. Energy. Combust. Sci.* **1988**, *14*, 1−98.

(42) Zeldovich, Y. B.; Barenblatt, G. I.; Librovich, V. B.; Makhviladze, G. M. *The Mathematical Theory of Combustion and Explosions*; Consultants Bureau: New York, 1985.

(43) Novozhilov, B. V. *Dokl. Akad. Nauk SSSR* **1961**, *141*, 151.

(44) Volpert, V. A.; Volpert, V. A.; Garbey, M.; Pojman, J. A. In *Gas-Phase Chemical Reaction Systems: Experiments and Models 100 Years after Max Bodenstein*; Wolfrum, J., Volpp, H.-R., Rannacher, R., Warnatz, J., Eds.; Springer: Berlin, Heidelberg, 1996; pp 309−317.

(45) Garbey, M.; Taik, A.; Volpert, V. *Q. Appl. Math.* **1996**, *54*, 225−247.

(46) Rayleigh, L. *Scientific Papers, ii*; Cambridge University Press: Cambridge, 1900.

(47) Taylor, G. *Proc. R. Soc. London, Ser. A* **1950**, *202*, 192−196.

(48) Pojman, J. A.; Curtis, G.; Ilyashenko, V. M. *J. Am. Chem. Soc.* **1996**, *115*, 3783−3784.

(49) Severs, E. T. *Rheology of Polymers*; Reinhold: New York, 1962.